

# The neutral curve for stationary disturbances in rotating disk flow for power-law fluids

P. T. Griffiths<sup>a,\*</sup>, S. J. Garrett<sup>b</sup>, S. O. Stephen<sup>c</sup>

<sup>a</sup>*School of Mathematics, University of Birmingham, Edgbaston, Birmingham B15 2TT, UK*

<sup>b</sup>*Department of Engineering, University of Leicester, University Road, Leicester LE1 7RH, UK*

<sup>c</sup>*School of Mathematics & Statistics, University of New South Wales, Sydney, NSW, 2052, Australia*

---

## Abstract

This paper is concerned with the convective instabilities associated with the boundary-layer flow due to a rotating disk. Shear-thinning fluids that adhere to the power-law relationship are considered. The neutral curves are computed using a sixth-order system of linear stability equations which include the effects of streamline curvature, Coriolis force and the non-Newtonian viscosity model. Akin to previous Newtonian studies it is found that the neutral curves have two critical values, these are associated with the type I upper-branch (cross-flow) and type II lower-branch (streamline curvature) modes. Our results indicate that an increase in shear-thinning has a stabilising effect on both the type I and II modes, in terms of the critical Reynolds number and growth rate. Favourable agreement is obtained between existing asymptotic predictions and the numerical results presented here.

---

\*Corresponding author. Tel.: +44 (0) 121 414 9051

*Email addresses:* [p.griffiths@pgr.bham.ac.uk](mailto:p.griffiths@pgr.bham.ac.uk) (P. T. Griffiths), [stephen.garrett@le.ac.uk](mailto:stephen.garrett@le.ac.uk) (S. J. Garrett), [s.stephen@unsw.edu.au](mailto:s.stephen@unsw.edu.au) (S. O. Stephen)

*Keywords:* Instability, Rotating disk flow, Power-law fluid, Neutral curve

---

## 1. Introduction

The stability and transition of the boundary-layer flow due to a rotating disk has attracted considerable interest in recent decades and continues to be an area of flourishing research. The pioneering study of Gregory et al. [1] contains the first observation of the stationary cross-flow vortices on a rotating disk. These instabilities were explained theoretically using a high Reynolds number linear stability analysis. Malik [2] presents the first comprehensive numerical study concerning the convective stationary disturbances, computing the curves of neutral stability using a sixth-order system of linear disturbance equations. Utilising a parallel-flow approximation as well as including the effects of streamline curvature and Coriolis force Malik demonstrates that there exists two distinct neutral branches. An upper-branch due to the cross-flow instability, termed type I and a lower-branch attributed to external streamline curvature, termed type II. These numerical results were verified by the linear asymptotic analysis of Hall [3]. He recovered the type I solution presented by Gregory et al. [1] (later corrected by Gajjar [4]) and showed that an additional short-wavelength mode exists, its structure being fixed by a balance between viscous and Coriolis forces. This mode corresponds directly to the type II branch.

Lingwood [5] investigated the role of absolute instability showing that the boundary-layer on a rotating disk of infinite extent is locally absolutely unstable at Reynolds numbers in excess of a critical value. The value of the critical Reynolds number agrees exceptionally well with experimental data,

leading to Lingwood's hypothesis that absolute instability plays a part in turbulent transition on the rotating disk. Subsequently, Davies and Carpenter [6] investigated the global behaviour of the absolute instability of the rotating disk boundary-layer. By direct numerical simulations of the linearised governing equations they were able to show that the local absolute instability does not produce a linear global instability, instead suggesting that convective behaviour eventually dominates at all the Reynolds numbers. Their conclusion was that absolute instability was not involved in the transition process through linear effects. More recently, Pier [7] demonstrated explicitly that a nonlinear approach is required to explain the self-sustained behaviour of the rotating disk flow. Using the result of Huerre and Monkewitz [8] that the presence of local absolute instability does not necessarily give rise to linear global instability; Pier suggested that the flow has a primary nonlinear global mode (fixed by the onset of the local absolute instability) which has a secondary absolute instability that triggers the transition to turbulence.

Extending the rotating disk theory Lingwood [9] and Lingwood and Garrett [10] considered the BEK system of rotating boundary-layer flows, named as such as it encompasses a family of rotating flows including the Bödewadt, Ekam and von Kármán boundary layers. They show that as the Rossby number increases the flows become increasingly unstable in both the convective and absolute senses. Noting that the onset of convective and absolute instability occurs almost simultaneously at very low Reynolds number in the Bödewadt boundary-layer. Numerous other studies have utilised and modified the numerical scheme employed by Lingwood [5]. Garrett and Peake [11] consider the stability and transition of the boundary-layer on a rotat-

ing sphere whilst Garrett et al. [12] investigate the cross-flow instability of the boundary-layer on a rotating cone. One particularly interesting extension, with respect to the von Kármán boundary-layer, is the temperature-dependent viscosity study of Jasmine and Gajjar [13]. The authors introduce a viscosity model based on an inverse linear function of temperature, controlled by the small parameter  $\epsilon$ . They conclude that the stability of the flow is particularly sensitive to changes in viscosity and even for small positive values of  $\epsilon$  the flow is much more unstable compared to the constant viscosity case defined by  $\epsilon = 0$ .

In the current paper we examine the linear convective instability of the boundary-layer on a rotating disk for power-law fluids. This work is essentially a development stemming from the linear asymptotic study of Griffiths et al. [14] who hypothesised that shear-thinning fluids may have a stabilising effect on the flow. Following the approach of Malik [2] we compute curves of neutral stability that can then be directly compared to the asymptotic predictions of Griffiths et al. [14]. A brief review of the inconsistencies regarding steady mean flow solutions for this problem is given by Griffiths et al. [14], and for the reasons outlined therein we restrict our attention to flows with moderate levels of shear-thinning. The interested reader is referred to Denier and Hewitt [15] for an in-depth analysis. In §2 the solution of the boundary-layer equations that give the steady mean flow profiles is described and the unsteady perturbation equations for the system are derived. The convective instability analysis is conducted in §3, where our theoretical predictions are compared with existing asymptotic results and linear convective growth rates are discussed. Finally, our conclusions are presented in §4.

## 2. Formulation

We consider the flow of a steady incompressible power-law fluid due to an infinite rotating plane located at  $z^* = 0$ . The plane rotates about the  $z^*$ -axis with angular velocity  $\Omega^*$ . The motion of the fluid is in the positive  $z^*$  direction, the fluid is infinite in extent and the only boundary is located at  $z^* = 0$ . In a rotating frame of reference the continuity and Navier-Stokes equations are expressed as

$$\nabla \cdot \mathbf{u}^* = 0, \quad (1a)$$

$$\frac{\partial \mathbf{u}^*}{\partial t^*} + \mathbf{u}^* \cdot \nabla \mathbf{u}^* + \Omega^* \times (\Omega^* \times \mathbf{r}^*) + 2\Omega^* \times \mathbf{u}^* = -\frac{1}{\rho^*} \nabla p^* + \frac{1}{\rho^*} \nabla \cdot \boldsymbol{\tau}^*. \quad (1b)$$

Here  $\mathbf{u}^* = (\tilde{U}^*, \tilde{V}^*, \tilde{W}^*)$  are the velocity components in cylindrical polar coordinates  $(r^*, \theta, z^*)$ ,  $t^*$  is time,  $\boldsymbol{\Omega}^* = (0, 0, \Omega^*)$  and  $\mathbf{r}^* = (r^*, 0, z^*)$ . The fluid density is  $\rho^*$  and  $p^*$  is the fluid pressure. For generalised Newtonian models, such as the power-law model, the stress tensor is given by

$$\boldsymbol{\tau}^* = \mu^* \dot{\boldsymbol{\gamma}}^* \quad \text{with} \quad \mu^* = \mu^*(\dot{\boldsymbol{\gamma}}^*),$$

where  $\dot{\boldsymbol{\gamma}}^* = \nabla \mathbf{u}^* + (\nabla \mathbf{u}^*)^T$  is the rate of strain tensor and  $\mu^*(\dot{\boldsymbol{\gamma}}^*)$  is the non-Newtonian viscosity. The magnitude of the rate of strain tensor is

$$\dot{\boldsymbol{\gamma}}^* = \sqrt{\frac{\dot{\boldsymbol{\gamma}}^* : \dot{\boldsymbol{\gamma}}^*}{2}}.$$

The governing relationship for  $\mu^*(\dot{\boldsymbol{\gamma}}^*)$  when considering a power-law fluid is

$$\mu^*(\dot{\boldsymbol{\gamma}}^*) = m^*(\dot{\boldsymbol{\gamma}}^*)^{n-1}, \quad (2)$$

where  $m^*$  is the consistency coefficient and  $n$  is the dimensionless power-law index, with  $n > 1$ ,  $n < 1$  corresponding to shear-thickening and shear-thinning fluids, respectively. For  $n = 1$  we recover the Newtonian viscosity model.

In the Newtonian limit an exact solution of (1) exists, as was first determined by von Kármán [16]. However, no such solution exists for flows with  $n \neq 1$ . It is only in the large Reynolds number limit that the leading order boundary-layer equations admit a similarity solution analogous to the exact Newtonian solution. The governing boundary-layer equations are

$$\frac{1}{r^*} \frac{\partial(r^* \tilde{U}_0^*)}{\partial r^*} + \frac{1}{r^*} \frac{\partial \tilde{V}_0^*}{\partial \theta} + \frac{\partial \tilde{W}_0^*}{\partial z^*} = 0, \quad (3a)$$

$$\begin{aligned} \frac{\partial \tilde{U}_0^*}{\partial t^*} + \tilde{U}_0^* \frac{\partial \tilde{U}_0^*}{\partial r^*} + \frac{\tilde{V}_0^*}{r^*} \frac{\partial \tilde{U}_0^*}{\partial \theta} + \tilde{W}_0^* \frac{\partial \tilde{U}_0^*}{\partial z^*} - \frac{(\tilde{V}_0^* + r^* \Omega^*)^2}{r^*} \\ = \frac{1}{\rho^*} \frac{\partial}{\partial z^*} \left( \tilde{\mu}^* \frac{\partial \tilde{U}_0^*}{\partial z^*} \right), \end{aligned} \quad (3b)$$

$$\begin{aligned} \frac{\partial \tilde{V}_0^*}{\partial t^*} + \tilde{U}_0^* \frac{\partial \tilde{V}_0^*}{\partial r^*} + \frac{\tilde{V}_0^*}{r^*} \frac{\partial \tilde{V}_0^*}{\partial \theta} + \tilde{W}_0^* \frac{\partial \tilde{V}_0^*}{\partial z^*} + \frac{\tilde{U}_0^* \tilde{V}_0^*}{r^*} + 2\Omega^* \tilde{U}_0^* \\ = \frac{1}{\rho^*} \frac{\partial}{\partial z^*} \left( \tilde{\mu}^* \frac{\partial \tilde{V}_0^*}{\partial z^*} \right), \end{aligned} \quad (3c)$$

$$\begin{aligned} \frac{\partial \tilde{W}_0^*}{\partial t^*} + \tilde{U}_0^* \frac{\partial \tilde{W}_0^*}{\partial r^*} + \frac{\tilde{V}_0^*}{r^*} \frac{\partial \tilde{W}_0^*}{\partial \theta} + \tilde{W}_0^* \frac{\partial \tilde{W}_0^*}{\partial z^*} = -\frac{1}{\rho^*} \frac{\partial \tilde{P}_1^*}{\partial z^*} \\ + \frac{1}{\rho^* r^*} \frac{\partial}{\partial r^*} \left( \tilde{\mu}^* r^* \frac{\partial \tilde{U}_0^*}{\partial z^*} \right) + \frac{1}{\rho^* r^*} \frac{\partial}{\partial \theta} \left( \tilde{\mu}^* \frac{\partial \tilde{V}_0^*}{\partial z^*} \right) + \frac{2}{\rho^*} \frac{\partial}{\partial z^*} \left( \tilde{\mu}^* \frac{\partial \tilde{W}_0^*}{\partial z^*} \right), \end{aligned} \quad (3d)$$

with the viscosity function  $\tilde{\mu}^*$  given by

$$\tilde{\mu}^* = m^* \left[ \left( \frac{\partial \tilde{U}_0^*}{\partial z^*} \right)^2 + \left( \frac{\partial \tilde{V}_0^*}{\partial z^*} \right)^2 \right]^{(n-1)/2}. \quad (3e)$$

Here  $(\tilde{U}_0^*, \tilde{V}_0^*, \tilde{W}_0^*)$  are the leading order velocity components and  $\tilde{P}_1^*$  is the leading order fluid pressure term.

We introduce the generalisation of the classic Newtonian similarity solution in order to solve for the steady mean flow relative to the disk. The dimensionless similarity variables are defined by

$$U(\eta) = \frac{\tilde{U}_0^*}{r^*\Omega^*}, \quad V(\eta) = \frac{\tilde{V}_0^*}{r^*\Omega^*}, \quad W(\eta) = \frac{\tilde{W}_0^*}{\chi^*}, \quad P(\eta) = \frac{\tilde{P}_1^*}{\rho^*\chi^{*2}}, \quad (4)$$

where

$$\chi^* = \left[ \frac{\nu^*}{r^{*1-n}\Omega^{*1-2n}} \right]^{1/(n+1)}.$$

Here  $(U, V, W)$  are the dimensionless radial, azimuthal and axial base flow velocities, respectively,  $P$  is the pressure and  $\nu^* = m^*/\rho^*$  is the kinematic viscosity. The dimensionless similarity coordinate is

$$\eta = \frac{r^{*(1-n)/(n+1)} z^*}{L^{*2/(n+1)}} \quad \text{where} \quad L^* = \sqrt{\frac{\nu^*}{\Omega^{*2-n}}},$$

is the non-dimensionalising lengthscale. Thus the base flow is determined from the following set of non-linear ordinary differential equations:<sup>1</sup>

$$2U + \frac{1-n}{n+1}\eta U' + W' = 0, \quad (5a)$$

$$U^2 - (V+1)^2 + \left( W + \frac{1-n}{n+1}\eta U \right) U' - (\mu U')' = 0, \quad (5b)$$

$$2U(V+1) + \left( W + \frac{1-n}{n+1}\eta U \right) V' - (\mu V')' = 0, \quad (5c)$$

$$P' + WW' - (\mu W')' + 2\mu'U + \frac{1-n}{n+1} [U(\eta W' - W) + 2\mu U'] = 0, \quad (5d)$$

where the primes denote differentiation with respect to  $\eta$  and

$$\mu = \left[ U'^2 + V'^2 \right]^{(n-1)/2}. \quad (5e)$$

---

<sup>1</sup>We note the difference between (5d) when compared with (A1) of Denier and Hewitt [15], using the notation of the authors, the term  $[(n-1)/(n+1)](\hat{\mu}F')'$  should be multiplied by  $-\eta$ , thus allowing for the above simplification.

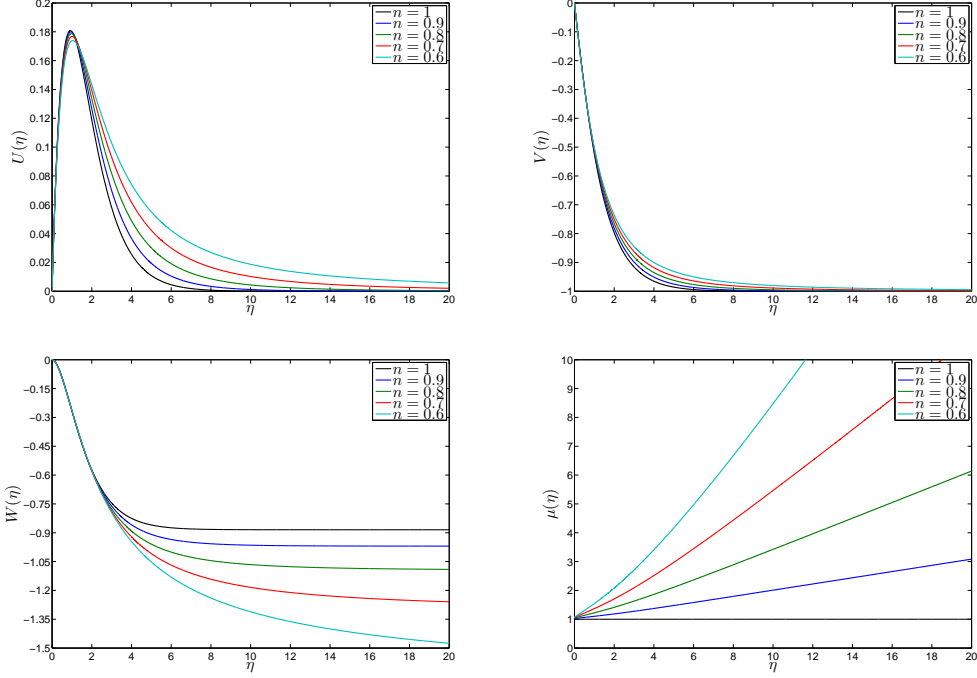


Figure 1: Plots of  $U$ ,  $V$ ,  $W$  and  $\mu$  versus  $\eta$  for  $n = 1, 0.9, 0.8, 0.7, 0.6$ . The  $\eta$ -axis has been truncated at  $\eta = 20$ .

Using a fourth-order Runge-Kutta quadrature routine twinned with a Newton iteration scheme to determine the values of the unknowns  $U'(0)$  and  $V'(0)$  the set of ordinary differential equations are solved subject to

$$U(0) = V(0) = W(0) = 0, \quad U(\eta \rightarrow \infty) \rightarrow 0, \quad V(\eta \rightarrow \infty) \rightarrow -1. \quad (6)$$

Denier and Hewitt [15] have shown that bounded solutions of (5) subject to (6) exist only in the shear-thinning case for  $n > 0.5$ , thus in this study we will consider flows with power-law index in the range  $0.5 < n \leq 1$ . In addition to this, for  $0.5 < n < 1$  we apply the asymptotic matching condition

$$(U', V') = \frac{n}{\eta(n-1)}(U, V) \quad \text{as } \eta \rightarrow \infty, \quad (7)$$

at some suitably large value of  $\eta = \eta_\infty \gg 1$ . In the Newtonian case (7) becomes singular, when  $n = 1$  the velocity functions decay exponentially, Cochran [17] showed that

$$(U', V') = W_\infty(U, V) \quad \text{as } \eta \rightarrow \infty,$$

where  $W_\infty = -2 \int_0^\infty U d\eta$ . Solutions for  $(U, V, W)$  and  $\mu$  are presented in Figure 1. Although the formulation here is different these results are an exact reproduction of those of Griffiths et al. [14].

The stability analysis, applied at a radius  $r_a^*$ , involves imposing infinitesimally small disturbances on the steady mean flow. The local Reynolds number is defined as

$$R = r_a^{*2/(n+1)} \left[ \frac{\Omega^{*2-n} L^*}{\nu^*} \right]^{2/(n+1)} = \left[ \frac{r_a^*}{L^*} \right]^{2/(n+1)} = r_a^{2/(n+1)}. \quad (8)$$

The non-dimensionalising velocity, pressure and time-scales are  $r_a^* \Omega^*$ ,  $\rho^* r_a^{*2} \Omega^{*2}$  and  $L^*/(\Omega^* r_a^*)$ , respectively. The leading order pressure terms in the radial and azimuthal momentum equations are retained, allowing for the inclusion of the disturbance pressure terms in the respective linear disturbance equations. The instantaneous non-dimensional velocities and pressure are given by

$$\tilde{U}_0(\eta, r, \theta, t) = \frac{r}{R^{(n+1)/2}} U(\eta) + u(r, \theta, \eta, t), \quad (9a)$$

$$\tilde{V}_0(\eta, r, \theta, t) = \frac{r}{R^{(n+1)/2}} V(\eta) + v(r, \theta, \eta, t), \quad (9b)$$

$$\tilde{W}_0(\eta, r, \theta, t) = \frac{r^{(n-1)/(n+1)}}{R^{(n+1)/2}} W(\eta) + w(r, \theta, \eta, t), \quad (9c)$$

$$\tilde{P}_1(\eta, r, \theta, t) = \frac{r^{2(n-1)/(n+1)}}{R^{(n+1)}} P(\eta) + p(r, \theta, \eta, t), \quad (9d)$$

where  $\eta = \eta(r, z) = r^{(1-n)/(n+1)}z$  and  $u, v, w$  and  $p$  are small perturbation quantities.

The dimensionless Navier-Stokes equations are linearised with respect to the perturbation quantities. In much the same way as Lingwood [5] we utilise a parallel-flow approximation in order to make the linearised perturbation equations separable in  $r, \theta$  and  $t$ . Ignoring variations in the Reynolds number with radius we replace the variable  $r$  with  $R^{(n+1)/2}$ . Hence the linear disturbance equations are

$$R^{(n-1)/2} \frac{\partial u}{\partial r} + \frac{u}{R} + \frac{\eta(1-n)}{R(n+1)} \frac{\partial u}{\partial \eta} + \frac{1}{R} \frac{\partial v}{\partial \theta} + \frac{\partial w}{\partial \eta} = 0, \quad (10a)$$

$$\begin{aligned} R^{(n-1)/2} \left( \frac{\partial u}{\partial t} + U \frac{\partial u}{\partial r} \right) + \frac{V}{R} \frac{\partial u}{\partial \theta} + \frac{W}{R} \frac{\partial u}{\partial \eta} + \frac{Uu}{R} - \frac{2(V+1)v}{R} + U'w \\ + \frac{\eta(1-n)}{R(n+1)} \left( U'u + U \frac{\partial u}{\partial \eta} + \frac{\partial p}{\partial \eta} \right) = -R^{(n-1)/2} \frac{\partial p}{\partial r} \\ + \frac{1}{R} \frac{\partial}{\partial \eta} \left( \mu \frac{\partial u}{\partial \eta} + \hat{\mu}U' \right), \quad (10b) \end{aligned}$$

$$\begin{aligned} R^{(n-1)/2} \left( \frac{\partial v}{\partial t} + U \frac{\partial v}{\partial r} \right) + \frac{V}{R} \frac{\partial v}{\partial \theta} + \frac{W}{R} \frac{\partial v}{\partial \eta} + \frac{Uv}{R} + \frac{2(V+1)u}{R} + V'w \\ + \frac{\eta(1-n)}{R(n+1)} \left( V'u + U \frac{\partial v}{\partial \eta} \right) = -\frac{1}{R} \frac{\partial p}{\partial \theta} + \frac{1}{R} \frac{\partial}{\partial \eta} \left( \mu \frac{\partial v}{\partial \eta} + \hat{\mu}V' \right), \quad (10c) \end{aligned}$$

$$\begin{aligned} R^{(n-1)/2} \left( \frac{\partial w}{\partial t} + U \frac{\partial w}{\partial r} \right) + \frac{V}{R} \frac{\partial w}{\partial \theta} + \frac{W}{R} \frac{\partial w}{\partial \eta} + \frac{W'w}{R} + \frac{\eta(1-n)}{R(n+1)} U \frac{\partial w}{\partial \eta} \\ = -\frac{\partial p}{\partial \eta} + \frac{1}{R} \frac{\partial}{\partial \eta} \left( \mu \frac{\partial w}{\partial \eta} \right) + O(R^{-2}). \quad (10d) \end{aligned}$$

The additional viscous terms  $\hat{\mu}U'$  and  $\hat{\mu}V'$  appear here due to the first-order cross-product terms associated with the generalised binomial expansion of the

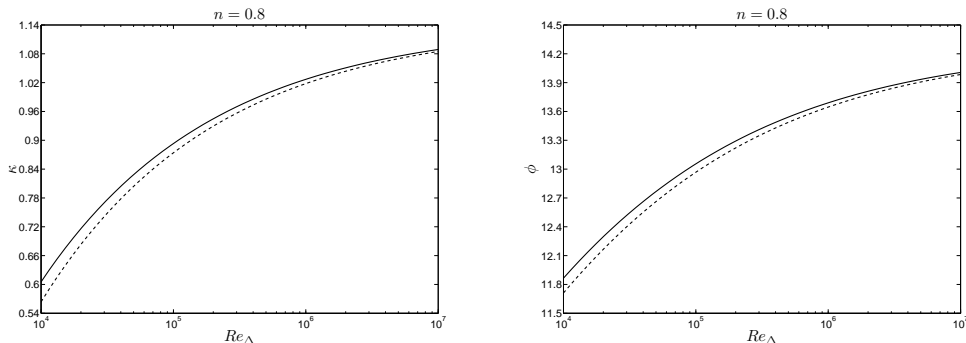


Figure 2: Plots of the asymptotic neutral wavenumber  $\kappa$  and wave angle  $\phi$  for  $n = 0.8$ . The solid lines are the analytical solutions of Griffiths et al. [14], the dashed lines represent the approximate solutions.

perturbed viscosity function (5e). The form of  $\hat{\mu}$  is given in the Appendix. No such terms appear in (10d) as these are found to be  $O(R^{-2})$ .

The  $O(R^{-2})$  terms are neglected, and as in the rotating cone study of Garrett et al. [12], we assume that  $\eta/R \ll 1$ . The aforementioned viscous terms are also removed from this study, we appeal to the asymptotic investigation of Griffiths et al. [14] for justification of this simplification. The authors have shown that inclusive of the disturbance viscosity terms  $\hat{\mu}(U', V')$ , analytical asymptotic solutions are obtainable when considering the upper-branch neutral modes for  $0.5 < n \leq 1$ . In order to investigate the effect these viscous terms have on the type I solutions an identical asymptotic study was undertaken, comparing the two sets of solutions, both with, and without the additional terms. It transpires that the solutions obtained from the reduced system of equations do provide an excellent approximation to those presented by Griffiths et al. [14]. Comparative plots of the asymptotic neutral wavenumber and wave angle are presented in Figure 2. Indeed, for

every  $n$  in the range of interest there is a good agreement between the two sets of solutions, with the limiting asymptotic values being recovered by the approximate results as  $R \rightarrow \infty$ , as observed in Figure 2.

Having simplified the linear disturbance equations we assume that the perturbation quantities have the normal-mode form

$$u = \hat{u}(\eta; \alpha, \beta, \omega; R, n)e^{i(\alpha r + \beta \theta - \omega t)}, \quad (11a)$$

$$v = \hat{v}(\eta; \alpha, \beta, \omega; R, n)e^{i(\alpha r + \beta \theta - \omega t)}, \quad (11b)$$

$$w = \hat{w}(\eta; \alpha, \beta, \omega; R, n)e^{i(\alpha r + \beta \theta - \omega t)}, \quad (11c)$$

$$p = \hat{p}(\eta; \alpha, \beta, \omega; R, n)e^{i(\alpha r + \beta \theta - \omega t)}, \quad (11d)$$

where  $\hat{u}$ ,  $\hat{v}$  and  $\hat{w}$  are the spectral representations of the perturbation velocities and  $\hat{p}$  is the spectral representation of the perturbation pressure. The frequency of the disturbance in the rotating frame is  $\omega$ , the complex radial wavenumber is  $\alpha = \alpha_r + i\alpha_i$  and  $\beta$  is the real azimuthal wavenumber.

The perturbation equations may be written as a set of six first order ordinary differential equations in the following transformed variables:

$$\eta_1(\eta; \alpha, \beta, \omega; R, n) = (\bar{\alpha} - i/R)\hat{u} + \bar{\beta}\hat{v}, \quad (12a)$$

$$\eta_2(\eta; \alpha, \beta, \omega; R, n) = (\bar{\alpha} - i/R)D\hat{u} + \bar{\beta}D\hat{v}, \quad (12b)$$

$$\eta_3(\eta; \alpha, \beta, \omega; R, n) = \hat{w}, \quad (12c)$$

$$\eta_4(\eta; \alpha, \beta, \omega; R, n) = \hat{p}, \quad (12d)$$

$$\eta_5(\eta; \alpha, \beta, \omega; R, n) = (\bar{\alpha} - i/R)\hat{v} - \bar{\beta}\hat{u}, \quad (12e)$$

$$\eta_6(\eta; \alpha, \beta, \omega; R, n) = (\bar{\alpha} - i/R)D\hat{v} - \bar{\beta}D\hat{u}, \quad (12f)$$

where  $\bar{\alpha} = R^{(n-1)/2}\alpha$ ,  $\bar{\beta} = \beta/R$  and  $D$  represents differentiation with respect

to  $\eta$ . These equations are

$$D\eta_1 = \eta_2, \quad (13a)$$

$$\left[ \frac{\mu D \eta_2}{R} \right]_v = \frac{\eta_2 (W_s - D\mu_v)}{R} + \frac{[iR(\bar{\alpha}U + \bar{\beta}V - \bar{\omega}) + U_s] \eta_1}{R} - \frac{2(1_c + V_s)\eta_5}{R} + (\bar{\alpha}_1 DU + \bar{\beta}DV)\eta_3 + i \left[ \kappa^2 - \left( \frac{\bar{\alpha}i}{R} \right)_s \right] \eta_4, \quad (13b)$$

$$D\eta_3 = -i\eta_1, \quad (13c)$$

$$D\eta_4 = \frac{i[\eta_1 W_s - D(\eta_1 \mu)_v]}{R} - \frac{[iR(\bar{\alpha}U + \bar{\beta}V - \bar{\omega}) + DW_s] \eta_3}{R}, \quad (13d)$$

$$D\eta_5 = \eta_6, \quad (13e)$$

$$\left[ \frac{\mu D \eta_6}{R} \right]_v = \frac{\eta_6 (W_s - D\mu_v)}{R} + \frac{[iR(\bar{\alpha}U + \bar{\beta}V - \bar{\omega}) + U_s] \eta_5}{R} + \frac{2(1_c + V_s)\eta_1}{R} + (\bar{\alpha}_1 DV - \bar{\beta}DU)\eta_3 + \left[ \frac{\bar{\beta}\eta_4}{R} \right]_s, \quad (13f)$$

where  $\bar{\omega} = R^{(n-1)/2}\omega$ ,  $\bar{\alpha}_1 = \bar{\alpha} - (i/R)_s$ ,  $\kappa^2 = \bar{\alpha}^2 + \bar{\beta}^2$  and the subscripts  $v$ ,  $c$  and  $s$  indicate which of the  $O(R^{-1})$  terms are the viscous, Coriolis and streamline curvature terms, respectively.

If the Coriolis and streamline curvature effects are neglected, the result can be written as the fourth-order Orr-Sommerfeld equation for the rotating disk

$$\begin{aligned} & [i(\mu D^2 + D\mu D)(D^2 - \kappa^2) + iD(D\mu D^2) \\ & + R(\bar{\alpha}U + \bar{\beta}V - \bar{\omega})(D^2 - \kappa^2) - R(\bar{\alpha}D^2U + \bar{\beta}D^2V)] \eta_3 = 0. \end{aligned} \quad (14)$$

Neglecting all the viscous terms the Orr-Sommerfeld equation reduces to the Rayleigh equation

$$[(\bar{\alpha}U + \bar{\beta}V - \bar{\omega})(D^2 - \kappa^2) - (\bar{\alpha}D^2U + \bar{\beta}D^2V)] \eta_3 = 0. \quad (15)$$

We note here that

$$\kappa = \sqrt{\bar{\alpha}^2 + \bar{\beta}^2} = r^{(n-1)/(n+1)} \sqrt{\alpha^2 + \frac{\beta^2}{r^2}},$$

$$\phi = \tan^{-1} \left( \frac{\bar{\beta}}{\bar{\alpha}} \right) \Leftrightarrow \tan \left( \frac{\pi}{2} - \phi \right) = \frac{\alpha r}{\beta},$$

thus the definitions of the neutral wavenumber and wave angle are consistent with that of Griffiths et al. [14].

Substitution of  $n = 1$  into (13) does not admit the Newtonian set of perturbation equations derived by Lingwood [5]. This is because of the boundary-layer approximation used in the formulation of this problem. In order to construct steady mean flow solutions the higher order viscous terms are removed, for details see Denier and Hewitt [15]. Thus we observe this slight departure from the expected Newtonian results<sup>2</sup>. We comment on the implications of this departure in §3. We do note however, that (13) does indeed reduce to the corresponding Newtonian system when considered in the frame of a boundary-layer approximation, as is to be expected.

### 3. Convective stability analysis

We solve the eigenvalue problem defined by system (13) subject to the boundary conditions

$$\eta_i = 0 \quad \text{at} \quad \eta = 0, \tag{16a}$$

$$\eta_i \rightarrow 0 \quad \text{as} \quad \eta \rightarrow \infty, \tag{16b}$$

---

<sup>2</sup>A comparison between the exact, Newtonian, perturbation equations and this system of boundary-layer equations is provided in the Appendix.

for  $i = 1, 2, \dots, 6$ . This eigenvalue problem will be solved for certain combinations of values of  $\alpha$ ,  $\beta$  and  $\omega$  at each Reynolds number,  $R$ , and for the specified value of  $n$ . From these we form the dispersion relation,  $D(\alpha, \beta, \omega; R, n) = 0$ , at each  $n$ , with the aim of studying the convective instabilities. The step size in  $\eta$  was reduced and the value of infinity increased until there were no discernible differences in the numerical results. The values taken were such that the boundary layer was approximated by 2000 equally spaced data points between  $\eta = 0$  and  $\eta = 20$ . This discretization is known to be consistent with Lingwood [5] and Garrett and Peake [18], for example, and represents an appropriate balance between accuracy and computational effort for each  $n$ .

The spatial branches are calculated using a double-precision fixed-step-size, fourth-order Runge-Kutta integrator with Gram-Schmidt orthonormalization and a Newton-Raphson linear search procedure, using a modification of the numerical code discussed in Garrett and Peake [11]. Solutions of the sixth-order system are dependent on the form (13) takes as  $\eta \rightarrow \infty$ . From Figure 1 we observe the viscosity function  $\mu$  tending to a constant gradient as  $\eta \rightarrow \infty$ . From the governing non-linear ODEs (5) we find that

$$\mu' \rightarrow \frac{(n-1)}{n} W_\infty \quad \text{as } \eta \rightarrow \infty, \quad (17)$$

where

$$W_\infty = -\frac{(3n+1)}{(n+1)} \int_0^\infty U \, d\eta.$$

Clearly this behaviour is unphysical, predicting that fluid is entrained into the boundary-layer with unbounded viscosity as the axial distance is increased, this being a result of the boundary-layer approximation mentioned previously. Here the boundary-layer is approximated by the region  $0 \leq \eta \leq 20$ ,

thus we find that generally the axial velocity component will not have converged to its constant limiting value within the confines of the boundary-layer region. This is due to the strong dependence the function  $W$  has on the fluid index  $n$  as it decays to the far-field, as noted by Denier and Hewitt [15]. Indeed, the computational boundary-layer thickness could be extended to ensure the use of fully converged steady mean flow results when solving system (13), however, this proves to be computationally very expensive. We find that increasing  $\eta_\infty$  beyond  $\eta_\infty = 20$  does not serve to provide any significantly more accurate results. Thus, in much the same way as the study of Garrett and Peake [18], we conclude that in this case, the cramping of the boundary-layer does not cause major inaccuracies when solving (13) subject to (16).

In order to investigate the structure of the spatial branches at each  $n$ , we solve the dispersion relation for  $\alpha$  whilst marching through values of  $\beta$  at fixed  $R$ . For each  $n$  in the particular range of interest two spatial branches determine the convective instability characteristics of the system. Figure 3 shows the structure of these two branches in the complex  $\alpha$ -plane when  $n = 0.8$  for  $R = 700$  and  $R = 745$ , we note that these plots have been constructed in the unscaled  $\alpha$  axes as opposed to the scaled  $\bar{\alpha}$  axes. A branch lying below the line  $\alpha_i = 0$  indicates convective instability. Branch 2 ceases to exist when analysing the Orr-Sommerfeld equation (14), indicating that it has to arise from streamline curvature effects. We observe from Figure 3 that at  $R = 745$  there has been an exchange of modes. The modified branch 1 now determines the region of convective instability. Increasing the value of  $R$  causes the peak between the two minima on branch 1 to move downwards

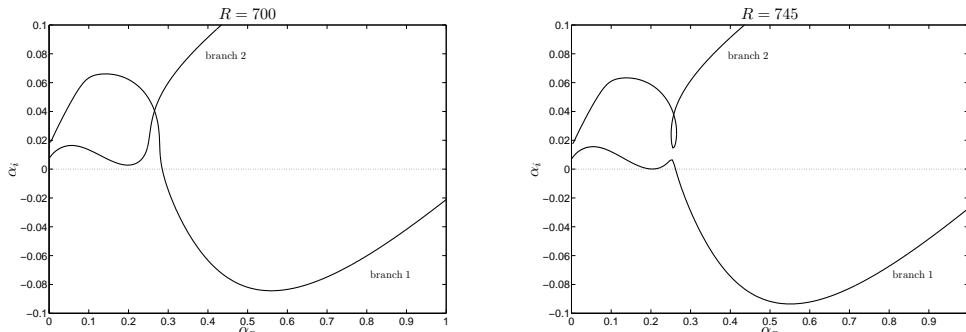


Figure 3: The two spatial branches for the case when  $n = 0.8$ , showing type I instability from branch 1 only at  $R = 700$  and type I and type II instabilities from the modified branch 1 at  $R = 745$ .

and the points where the branch crosses the line  $\alpha_i = 0$  move apart, thereby widening the regions of instability and mapping out two lobes on the neutral curve. Above a certain value of  $R$  the peak moves below the line  $\alpha_i = 0$  and further increases in  $R$  change the region of instability, producing the upper and lower branches of the neutral curve.

This spatial branch behaviour is typical for each  $n$ . Neutral curves, defined by  $\alpha_i = 0$ , have been calculated for values of the power-law index ranging from  $n = 0.6 - 1$  in increments of 0.1. Figure 4 shows in detail the characteristic two-lobed structure synonymous with flows of this nature, an upper lobe due to the cross-flow instability and a lower lobe attributed to external streamline curvature. Each curve encloses a region that is convectively unstable. The neutral curves show that decreasing the power-law index has a stabilising effect on the boundary-layer flow. The value of the critical Reynolds number is increased on both the upper and lower lobes as  $n$  decreases, as shown in Tables 1 and 2, respectively. We note a slight

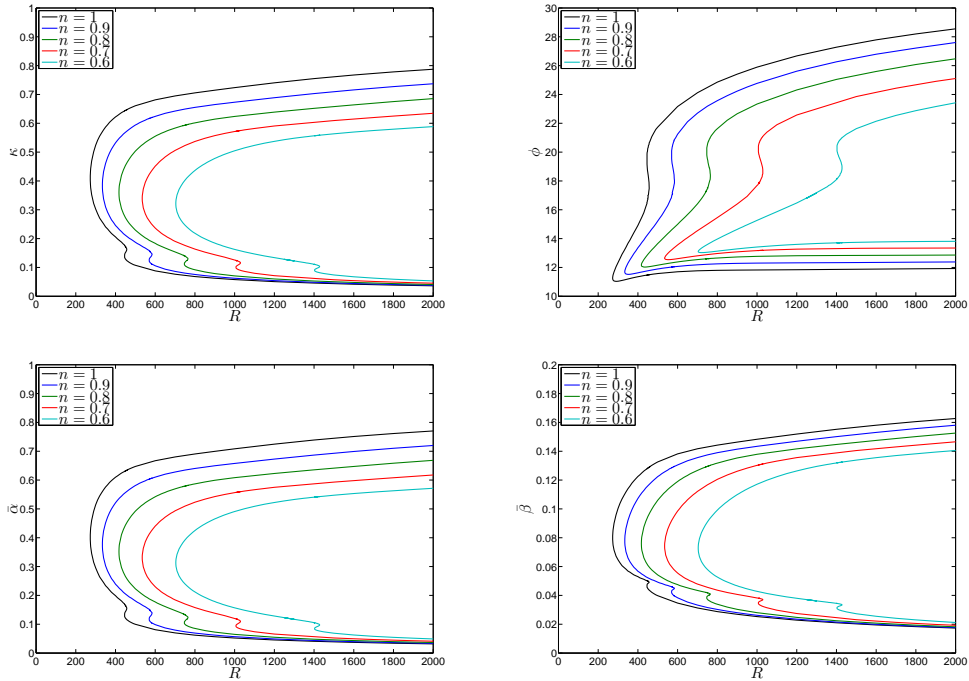


Figure 4: Neutral stability curves for decreasing values of  $n$ . The neutral, radial and azimuthal wave numbers and wave angle are plotted against the Reynolds number. The  $R$ -axis has been truncated at  $R = 2000$ .

discrepancy between our boundary-layer results for the case when  $n = 1$  and the exact Newtonian results ( $\epsilon = 0$ ) of Jasmine and Gajjar [13]. On the upper-branch Jasmine and Gajjar [13] report critical values of  $R = 287.2$  with  $\kappa = 0.3927$  and  $\phi = 11.40^\circ$  whilst on the lower-branch the critical values are given as  $R = 451.4$  with  $\kappa = 0.1402$  and  $\phi = 19.50^\circ$ . In both cases the value of the critical Reynolds number presented here is marginally reduced due to the inaccuracies associated with the boundary-layer approximation at these relatively small Reynolds numbers. As mentioned previously this boundary-layer approximation is necessary in order to construct steady mean

Table 1: The values of the critical Reynolds number  $R$ , wavenumbers  $\bar{\alpha}$ ,  $\bar{\beta}$  and  $\kappa$ , and wave angle  $\phi$  corresponding to decreasing values of  $n$  on the upper-branch for stationary waves.

$n$	$R$	$\bar{\alpha}$	$\bar{\beta}$	$\kappa$	$\phi$
1	272.90	0.4033	0.0802	0.4112	11.25°
0.9	334.01	0.3767	0.0780	0.3847	11.69°
0.8	417.49	0.3522	0.0759	0.3603	12.17°
0.7	534.55	0.3311	0.0743	0.3394	12.64°
0.6	703.77	0.3132	0.0729	0.3216	13.10°

Table 2: The values of the critical Reynolds number  $R$ , wavenumbers  $\bar{\alpha}$ ,  $\bar{\beta}$  and  $\kappa$ , and wave angle  $\phi$  corresponding to decreasing values of  $n$  on the lower-branch for stationary waves.

$n$	$R$	$\bar{\alpha}$	$\bar{\beta}$	$\kappa$	$\phi$
1	445.22	0.1322	0.0467	0.1402	19.46°
0.9	569.27	0.1183	0.0425	0.1257	19.77°
0.8	746.23	0.1054	0.0385	0.1122	20.04°
0.7	1006.3	0.0941	0.0347	0.1003	20.23°
0.6	1402.0	0.0845	0.0312	0.0901	20.28°

flow solutions when  $n \neq 1$ . We observe that although the critical Reynolds numbers have been reduced the values of the wavenumber and wave angle at these Reynolds numbers is not greatly affected when compared to the exact Newtonian results of Jasmine and Gajjar [13].

Figure 5 shows a comparison between the numerical results presented here and the asymptotic results of Griffiths et al. [14]. The wavenumber plots are on the left with the wave angle plots on the right. An excellent quantitative agreement is found between the two sets of solutions for each  $n$  in the range of interest. As expected, in the large Reynolds number limit, the asymptotic predictions are indeed very good. However, as the Reynolds number decreases we find that the asymptotic predictions stray somewhat from the numerical results. This will be discussed further in the concluding section.

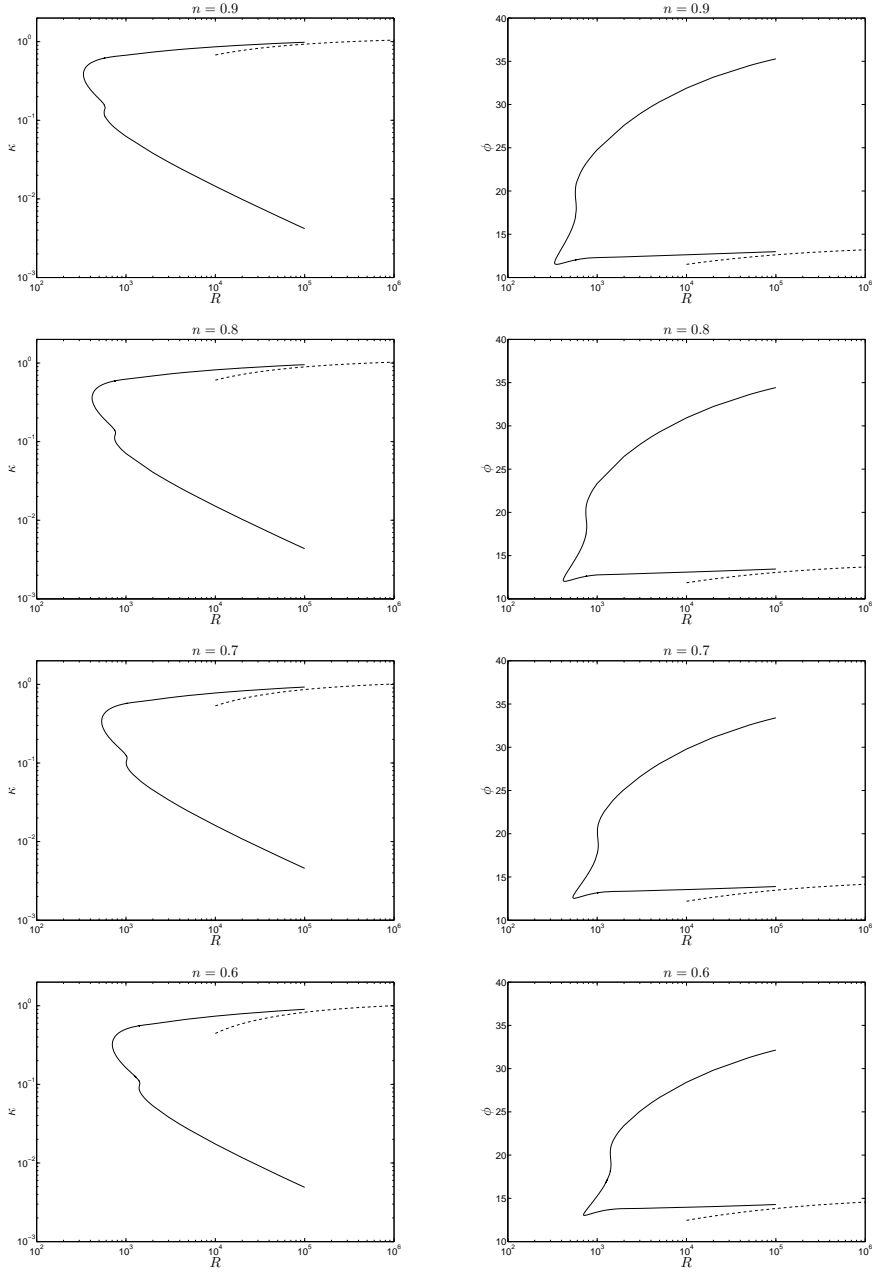


Figure 5: Neutral stability curves for  $n = 0.9, 0.8, 0.7, 0.6$ . The type I asymptotic solutions of Griffiths et al. [14] are given by the dashed lines.

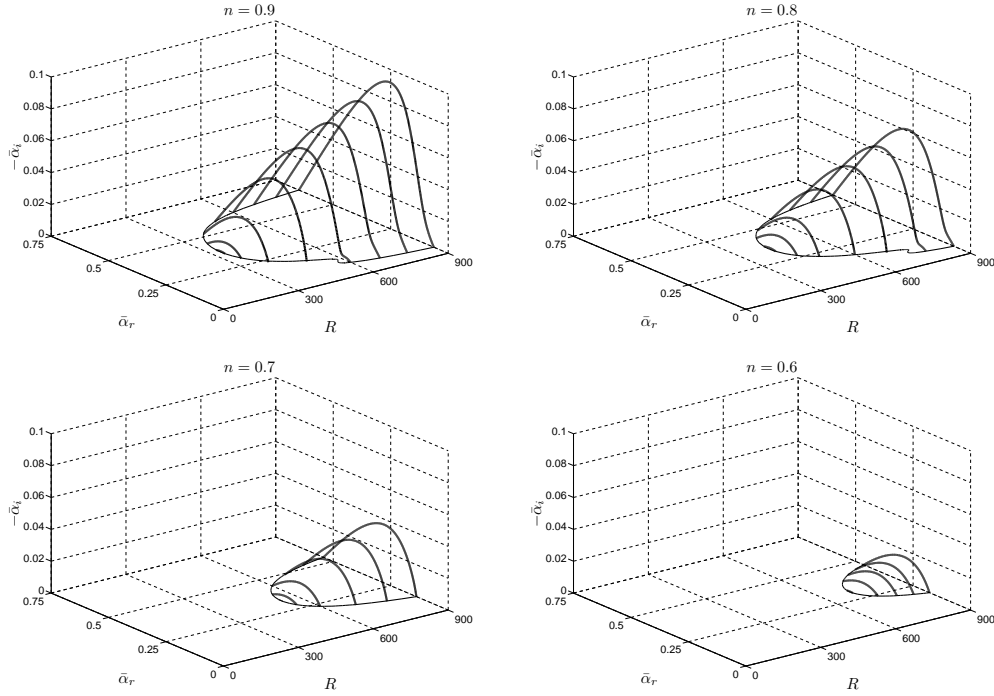


Figure 6: Linear convective growth rates for stationary mode disturbances of type I through the convectively unstable region for  $n = 0.9, 0.8, 0.7, 0.6$ .

Figure 6 plots the spatial branches of the type I mode through the convectively unstable region for decreasing values of  $n$  in order to visualize the growth rates. For clarity and brevity the type II growth rates are not included here. However, we find that on both the upper and lower branches, as  $n$  decreases the growth rates are significantly reduced whilst also being pushed to a higher critical Reynolds number, thus reaffirming the stabilising effect shear-thinning fluids have on the boundary-layer flow.

## 4. Conclusions

In this paper we have demonstrated that the stationary convective instabilities, associated with rotating disk flows, are amenable to numerical investigation when considering fluids that adhere to the power-law relationship. By reformulating the derivation of the base flow velocities we have constructed a new sixth-order system of linear stability equations dependent on the power-law index. The results presented in this study help to confirm previous suggestions that shear-thinning fluids have a stabilising effect on the flow, see Griffiths et al. [14] for details. We find that on both the type I and II modes the onset of linear convective instability is delayed as  $n$  decreases, the critical Reynolds number is increased and the linear convective growth rates are significantly reduced. Furthermore, a decrease in  $n$  results in the wavenumber and wave angle neutral curves undergoing a shift from the left to the right, effectively expanding the region of stable flow.

Direct comparisons have been made between the upper-branch asymptotic predictions of Griffiths et al. [14] and the wavenumber and wave angle neutral stability curves. There is an excellent agreement for all  $n$  in the large Reynolds number limit. A necessary asymptotic assumption is that  $R \gg 1$ . Thus the validity of these results diminishes somewhat as  $R$  decreases, hence we observe the slight departure from the numerical solutions in this case.

Two important approximations have been made during the completion of this work, we discuss these here. Firstly, instead of considering the full-field equations one must appeal to a boundary-layer approximation in order to obtain steady mean flow solutions. This has an effect on the ensuing derivation of the sixth-order system of linear stability equations. Consequently,

we find that reduction of this system to Newtonian form does not admit the governing equations stated by Lingwood [5], instead a number of minor simplifications are observed. As a result the formulation of the Orr-Sommerfeld equation (14) is also modified. However, when solving for the case  $n = 1$  we find that the results are comparable to those of previous Newtonian studies. Essentially use of the boundary-layer approximation decreases the critical Reynolds number on the type I and II modes predicting an advancement of the onset of linear convective instability. Thus, in the Newtonian case at least, the results presented here are considered to be less stable than those derived from the system of full-field equations. Secondly, in order to simplify the linear disturbance equations (10) a parallel-flow approximation was made and the disturbance viscosity terms  $\hat{\mu}(U', V')$  were removed. Having appealed to the asymptotic investigation of Griffiths et al. [14] we demonstrated that at high Reynolds number the type I neutral modes are not greatly effected by the removal of these additional viscous terms. Because of this and the parallel-flow approximation the perturbation equations solved in this analysis are not rigorous at  $O(R^{-1})$ . Although it is acknowledged that these approximations will lead to inaccuracies at the predicted critical Reynolds numbers, it is the authors' opinion that these will be small. The excellent agreement obtained between the numerical and exact asymptotic results shows that the affects of these approximations are negligible at high Reynolds number.

There are a number of limitations of the current study; we have considered only linear stationary convective instabilities. It would be of particular interest to investigate non-stationary modes ( $\omega \neq 0$ ) of instability thus al-

lowing for a comparison between the spatial growth rates of stationary and non-stationary modes. In addition to this an absolute instability analysis would provide predictions of critical Reynolds numbers for the onset of absolute instability. We suggest that the stabilising nature of shear-thinning fluids as noted here would again be observed when considering an absolute instability analysis. Furthermore, this investigation only encompasses fluids with a power-law index in the range  $0.5 < n \leq 1$ . The results presented here could be reproduced for shear-thickening fluids ( $n > 1$ ) since the derivation of the perturbation equations holds for all  $n > 0$ , although due care and attention needs to be given to the steady mean flow solutions in this case, the interested reader is referred to Denier and Hewitt [15]. Beyond a critical level of shear-thinning ( $n \leq 0.5$ ) the steady mean flow solutions grow in the far-field, so cannot be matched to the external flow. Thus a numerical solution of the governing non-linear partial differential equations is required; this is outside the scope of the current study.

Besides the above directions, there are other areas for future work on this problem. The lower-branch stationary modes could also be studied asymptotically. It would be advantageous to be able to compare these predictions with our numerical results. Indeed initial investigations into this problem have begun; we hope to report on this study in due course.

## **Acknowledgments**

PTG gratefully acknowledges the support of the Engineering and Physical Sciences Research Council UK for his PhD studies.

## Appendix A. Disturbance viscosity function

The disturbance viscosity function  $\hat{\mu}$  is given by

$$\hat{\mu} = \frac{(n-1)\mu}{U'^2 + V'^2} \left( U' \frac{\partial u}{\partial \eta} + V' \frac{\partial v}{\partial \eta} \right). \quad (\text{A.1})$$

We note that the above is directly equivalent to the function  $\bar{\mu}$  given in (19) of Griffiths et al. [14].

## Appendix B. Perturbation equations

Lingwood [5] gives the exact Newtonian perturbation equations as

$$D\eta_1 = \eta_2, \quad (\text{B.1})$$

$$\begin{aligned} \left[ \frac{D\eta_2}{R} \right]_v &= \frac{\eta_2 W_s}{R} + \frac{[\kappa_v^2 + iR(\bar{\alpha}U + \bar{\beta}V - \bar{\omega}) + U_s] \eta_1}{R} \\ &\quad - \frac{2(1_c + V_s)\eta_5}{R} + (\bar{\alpha}_1 DU + \bar{\beta}DV)\eta_3 + i \left[ \kappa^2 - \left( \frac{\bar{\alpha}i}{R} \right)_s \right] \eta_4, \end{aligned} \quad (\text{B.2})$$

$$D\eta_3 = -i\eta_1, \quad (\text{B.3})$$

$$D\eta_4 = \frac{i[\eta_1 W_s - D(\eta_1)_v]}{R} - \frac{[\kappa_v^2 + iR(\bar{\alpha}U + \bar{\beta}V - \bar{\omega}) + DW_s] \eta_3}{R}, \quad (\text{B.4})$$

$$D\eta_5 = \eta_6, \quad (\text{B.5})$$

$$\begin{aligned} \left[ \frac{D\eta_6}{R} \right]_v &= \frac{\eta_6 W_s}{R} + \frac{[\kappa_v^2 + iR(\bar{\alpha}U + \bar{\beta}V - \bar{\omega}) + U_s] \eta_5}{R} \\ &\quad + \frac{2(1_c + V_s)\eta_1}{R} + (\bar{\alpha}_1 DV - \bar{\beta}DU)\eta_3 + \left[ \frac{\bar{\beta}\eta_4}{R} \right]_s, \end{aligned} \quad (\text{B.6})$$

The  $\kappa_v^2$  terms vanish when appealing to a boundary-layer approximation. Thus we see that substitution of  $n = 1$  into (13) does admit the corresponding Newtonian boundary-layer set of perturbation equations.

## References

- [1] N. Gregory, J. T. Stuart, W. S. Walker, On the stability of three-dimensional boundary layers with applications to the flow due to a rotating disk, *Phil. Trans. R. Soc. Lond. A* 248 (1955) 155–199.
- [2] M. R. Malik, The neutral curve for stationary disturbances in rotating-disk flow, *J. Fluid Mech.* 164 (1986) 275–287.
- [3] P. Hall, An asymptotic investigation of the stationary modes of instability of the boundary layer on a rotating disc, *Proc. R. Soc. Lond. A* 406 (1986) 93–106.
- [4] J. S. B. Gajjar, Nonlinear critical layers in the boundary layer on a rotating disk, *J. Eng. Math.* 57 (2007) 205–217.
- [5] R. J. Lingwood, Absolute instability of the boundary layer on a rotating disk, *J. Fluid Mech.* 299 (1995) 17–33.
- [6] C. Davies, P. W. Carpenter, Global behaviour corresponding to the absolute instability of the rotating-disk boundary layer, *J. Fluid Mech.* 486 (2003) 287–329.
- [7] B. Pier, Finite-amplitude crossflow vortices, secondary instability and transition in the rotating-disk boundary layer, *J. Fluid Mech.* 487 (2003) 315343.
- [8] P. Huerre, P. A. Monkewitz, Local and global instabilities in spatially developing flows, *Annu. Rev. Fluid Mech.* 22 (1990) 473537.

- [9] R. J. Lingwood, Absolute instability of the Ekman layer and related rotating flows, *J. Fluid Mech.* 331 (1997) 405–428.
- [10] R. J. Lingwood, S. J. Garrett, The effects of surface mass flux on the instability of the BEK system of rotating boundary-layer flows, *Euro. J. Mech. B* 30 (2011) 299–310.
- [11] S. J. Garrett, N. Peake, The stability and transition of the boundary layer on a rotating sphere, *J. Fluid Mech.* 456 (2002) 199–218.
- [12] S. J. Garrett, Z. Hussain, S. O. Stephen, The cross-flow instability of the boundary layer on a rotating cone, *J. Fluid Mech.* 422 (2009) 209–232.
- [13] H. A. Jasmine, J. S. B. Gajjar, Absolute and convective instabilities in the incompressible boundary layer on a rotating disk with temperature-dependent viscosity, *Int. J. Heat Mass Transfer* 48 (2005) 1022–1037.
- [14] P. T. Griffiths, S. O. Stephen, A. P. Bassom, S. J. Garrett, Stability of the boundary layer on a rotating disk for power law fluids, *J. Non-Newtonian Fluid Mech.* 207 (2014) 1–6.
- [15] J. P. Denier, R. E. Hewitt, Asymptotic matching constraints for a boundary-layer flow of a power-law fluid, *J. Fluid Mech.* 518 (2004) 261–279.
- [16] T. von Kármán, Über laminare und turbulente Reibung, *Z. Angew. Math. Mech.* 1 (1921) 233–252.
- [17] W. G. Cochran, The flow due to a rotating disk, *Proc. Camb. Phil. Soc.* 30 (1934) 365–375.

- [18] S. J. Garrett, N. Peake, The stability of the boundary layer on a rotating sphere in a uniform axial flow, *Euro. J. Mech. B* 23 (2004) 241–253.